Quasiparticle band gap of organic-inorganic hybrid perovskites: Crystal structure, spin-orbit coupling, and self-energy effects

Weiwei Gao, Xiang Gao, Tesfaye A. Abtew, Yi-Yang Sun, Shengbai Zhang, and Peihong Zhang

Quasiparticle band gap of organic-inorganic hybrid perovskites: Crystal structure, spin-orbit coupling, and self-energy effects

Weiwei Gao[1], Xiang Gao[2], Tesfaye A. Abtew[1], Yi-Yang Sun[3], Shengbai Zhang[3], and Peihong Zhang[1,2*]

[1]*Department of Physics, University at Buffalo, State University of New York, Buffalo, New York 14260, USA*
[2]*Beijing Computational Science Research Center, Beijing 100084, China*
[3]*Department of Physics, Applied Physics and Astronomy,*
Rensselaer Polytechnic Institute, Troy, New York 12180, USA

(Dated: January 26, 2016)

The quasiparticle band gap is one of the most important materials properties for photovoltaic applications. Often the band gap of a photovoltaic material is determined (and can be controlled) by various factors, complicating predictive materials optimization. An in-depth understanding of how these factors affect the size of the gap will provide valuable guidance for new materials discovery. Here we report a comprehensive investigation on the band gap formation mechanism in organic-inorganic hybrid perovskites by decoupling various contributing factors which ultimately determine their electronic structure and quasiparticle band gap. Major factors, namely, quasiparticle self-energy, spin-orbit coupling, and structural distortions due to the presence of organic molecules, and their influences on the quasiparticle band structure of organic-inorganic hybrid perovskites are illustrated. We find that although methylammonium cations do not contribute directly to the electronic states near band edges, they play an important role in defining the band gap by introducing structural distortions and controlling the overall lattice constants. The spin-orbit coupling effects drastically reduce the electron and hole effective masses in these systems, which is beneficial for high carrier mobilities and small exciton binding energies.

I. INTRODUCTION

Organometal hybrid perovskite materials of the form ABX_3 (A: organic cations; B: Pb or Sn; X: iodine or other halogens) have emerged as one of the most promising light absorbers for thin-film solar cell applications. Among organic-inorganic perovskite materials, methylammonium mix triiodide ($CH_3NH_3PbI_{3-x}Cl_x$) has been shown to achieve an energy conversion efficiency of over 19%[1,2] and a relatively high open-circuit voltage of 1.1 V.[3] The high conversion efficiency of these materials has been attributed to their excellent photo-absorption coefficient,[4] high carrier mobility and long diffusion length,[5–7] and small exciton binding energy.[8,9] Unfortunately, so far the highest conversion efficiency is only achieved in Pb-containing systems. This is a major issue that needs to be addressed before these materials can be deployed at commercial scales. As a result, much recent effort has been devoted to the search for related Pb-free materials.[10–14]

The structural and chemical flexibility of these materials offer ample opportunities for materials design and optimization. For example, the band gap and optical absorption can be optimized/tuned by several factors such as the chemical compositions of the inorganic framework,[15–17] the organic cations,[17–19] and lattice strains possibly induced by substrates.[10] However, this rich design space also brings substantial complexity as multiple degrees of freedom may play distinct roles or may couple with each other to ultimately determine the optical properties of these materials. Therefore, an in-depth understanding of the excited states properties of these materials and how they are affected by various factors are critical for a theory-guided rational design or optimization.

First-principles GW methods[20] are highly accurate and theoretically well-based for predicting quasiparticle properties (i.e., charge excitations) of solids. In this paper, we analyze various factors that affect the electronic structure of hybrid perovskite materials including both the quasiparticle self-energy and the spin-orbit coupling (SOC) effects. Since the optically-relevant electronic states are derived mostly from the inorganic framework, we first investigate the electronic structure of ideal cubic phase, with and without the organic molecule. This study provides a clear understanding of the quasiparticle self-energy and SOC effects on the electronic properties of the optically active inorganic component, and the effect of organic molecule without structural distortions. Structural distortion and lattice (volume) effects are then investigated.

II. COMPUTATIONAL DETAILS

$CH_3NH_3PbI_3$ (MAPbI$_3$) has three different phases; the most studied ones are the high temperature (above 327 K) cubic phase with space group $Pm\bar{3}m$[21] (shown in Fig.1(a)) and the room temperature tetragonal phase with space group $I4/mcm$[21] (shown in Figure 1(c)). We will focus our investigation on these two phases. In both phases, the organic molecules are enclosed by eight corner-sharing octahedra and have no preferred orientations.[22–24] The tetragonal phase is slightly elongated along the c-axis and has an $a^0a^0c^-$ tilt of the PbI$_6$ octahedra, which can be seen clearly by comparing the top views (along the [001] direction) of the two phases as shown in Fig.1(b) and (d). We use the experimental

lattice constants[25,26] for all electronic structure calculations.
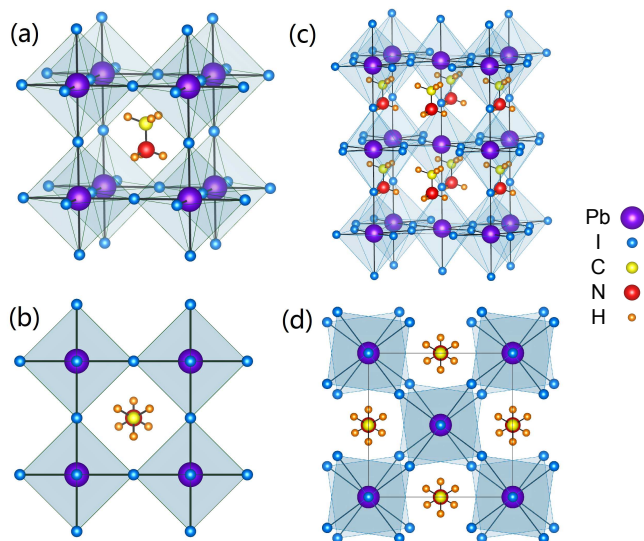
FIG. 1: (Color online) Crystal structures of the MAPbI$_3$. (a) and (b): cubic phase; (c) and (d): tetragonal phase.

The density functional theory (DFT)[27] calculations are carried out using plane-wave based methods implemented in `QUANTUM-ESPRESSO`[28] and `PARATEC`[29]. The Perdew-Burke-Ernzerhof (PBE) exchange-correlation functional[30] is used to account for the exchange-correlation effects, and norm-conserving pseudopotentials[31] are used for all calculations. A relatively high plane-wave kinetic energy cut-off of 60 Ry is applied to ensure the convergence of the calculated results since we use norm-conserving pseudopotentials. The Brillouin-zone integration is carried out on a $6 \times 6 \times 6$ Monkhorst-Pack grid[32] for cubic unit cells, and a similar k-point density is used for larger unit cells.

The quasiparticle calculations are carried out within the G^0W^0 approximation using a modified version of the `BerkeleyGW`[33] code to include SOC effects as first-order perturbation[34] to the quasiparicle properties. There have been previous reports on GW calculations with SOC effects,[35–38] our method is similar to that proposed by Malone and Cohen.[38] Specifically, the quasiparticle Hamiltonian including SOC effects is given by

$$
\begin{aligned}
H &= H_{\text{KS}} + (\Sigma^{\text{GW}} - V_{xc}) + \Delta^{\text{SOC}} \\
&= H_{\text{KS}} + \Delta^{\text{GW}} + \Delta^{\text{SOC}},
\end{aligned} \tag{1}
$$

where H_{KS} is the Kohn-Sham (KS) Hamiltonian, Δ^{GW} is the quasiparticle self energy correction within the GW approximation, and Δ^{SOC} is the SOC correction. We first carry out conventional GW calculations without SOC effects within the diagonal G^0W^0 approach.[20] The matrix elements of the SOC perturbation are evaluated using the KS eigenstates as a basis. The full Hamiltonian matrix

including both the self-energy and SOC effects becomes

$$
\begin{aligned}
H_{n,m}(\mathbf{k}) &= \langle n\mathbf{k}, \sigma_1 | H | m\mathbf{k}, \sigma_2 \rangle \\
&= \delta_{\sigma_1,\sigma_2} \delta_{n,m} E^{\text{GW}}_{n\mathbf{k},\sigma_1} + \langle n\mathbf{k}, \sigma_1 | \Delta^{\text{SOC}} | m\mathbf{k}, \sigma_2 \rangle,
\end{aligned}
$$

where σ_1, σ_2 are spin indexes, and n, m are band indexes. Diagonalizing the above Hamiltonian thus gives quasiparticle energies $E^{\text{GW+SOC}}_{n\mathbf{k}}$ and eigenvectors,

$$
|n\mathbf{k}, \alpha\rangle^{\text{GW+SOC}} = \sum_i \sum_{\sigma=\uparrow,\downarrow} b_{n\alpha,i\sigma}(\mathbf{k}) |i\mathbf{k}, \sigma\rangle^{\text{KS}}. \tag{2}
$$

This approach has been shown to give accurate results for semiconductors.[38]

We have carefully checked the convergence[39,40] of our GW calculations with respect to various cut-off parameters. Figure 2 shows the convergence behavior of the calculated GW band gap of the inorganic framework PbI$_3^-$ (without including SOC effects) with respect to the kinetic energy cut-off ($E_{cut} = \hbar^2 G_{cut}^2/2m$) for the dielectric matrix $\epsilon_{GG'}$ and the number of conduction bands included in the Coulomb-hole self-energy summation. It is clear that about 1000 bands are needed to converge the band gap to within 0.02 eV. In addition, a kinetic energy cut-off of at least 15 Ry is needed while calculating the dielectric matrix. All results reported in this work are calculated with higher convergence criteria, i.e., with a 30 Ry kinetic energy cut-off for the dielectric matrix and including 1500 bands in the Coulomb hole summation for the primitive cell of the cubic phase. We mention that for achieving the same level of convergence the required number of bands in GW calculations scales linearly with system size.
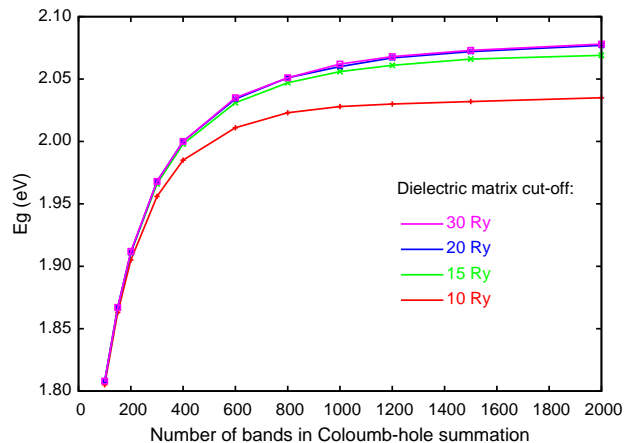
FIG. 2: (Color online) Convergence behavior of the calculated quasiparticle band gap as a function of the number of conduction bands included in the Coulomb-hole self-energy summation and the kinetic energy cut-off for the dielectric matrix.

The quasiparticle band structures presented in this work are obtained by interpolating the quasiparticle energies calculated on a uniform k-grid using the Wannier interpolation scheme.[41,42] The Wannier orbitals are

constructed using the KS eigenstates calculated on a $6 \times 6 \times 6$ uniform grid. All relevant atomic orbitals (i.e., I $5p$ and Pb $6s$, $6p$) are included in the initial projections of the KS states. A disentanglement method proposed by Souza *et al.*[42] is used. After constructing the Wannier orbitals and obtaining the relevant matrix elements, we can then calculate the interpolated band structures, with or without the GW and/or SOC corrections. Figure 3 compares the interpolated band structure and the calculated one for the cubic PbI_3^- framework within DFT, which shows the quality of the Wannier interpolation method.
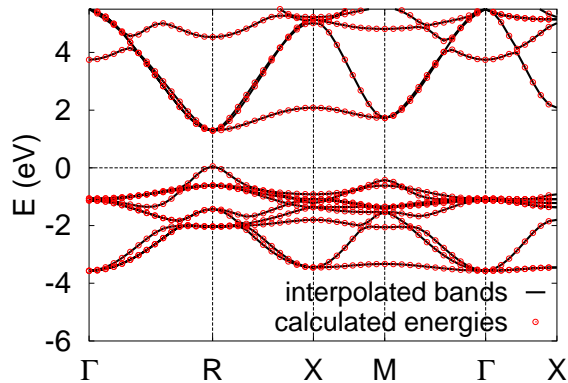
FIG. 3: (Color online) Comparision between the band structure calculated directly and that obtained by Wannier interpolation.

The effective masses are obtained using a least-square fitting procedure. We have calculated both the longitudinal ($R \rightarrow \Gamma$ direction) and transverse effective (perpendicular to $R \rightarrow \Gamma$ direction) masses near the R point where band extrema locate. At the DFT level, we calculate directly the band structure near the R point within a Δk of a few percent of the size of the Brillouin zone, and perform a least-squares fitting of the band structure within Δk from the R point. In terms of the energy range, the fittings are carried out over an energy window of about 0.1 eV from the band extrema. At the GW level, the effective masses are calculated using the Wannier-interpolated band structures.

III. RESULTS AND DISCUSSIONS

A. BASIC ELECTRONIC STRUCTURE

To understand and separate various effects on the electronic structure of $MAPbI_3$, we first discuss briefly the basic features of the band structures of cubic inorganic framework PbI_3^- and the unrelaxed cubic $CH_3NH_3PbI_3$ (with the organic molecule pointing along the [001] direction) using the experimental lattice constant.[25] We use the unrelaxed structure for $MAPbI_3$ here to illustrate the electronic effects of MA molecules; relaxation effects

due to the presence of organic molecules are discussed later. Figure 4 compares the band structures of cubic PbI_3^- (green dashed lines) and cubic $MAPbI_3$ (black solid lines) with the corresponding projected density of states (PDOS) calculated using the PBE functional. The DFT band gap of PbI_3^- is 1.24 eV, and that of $MAPbI_3$ is about 0.1 eV larger. Note that quasiparticle self-energy and SOC effects are not included at this point.

It is evident that the organic molecule has little effects on the band-edge states if the ideal crystal structure is used. The valence band maximum (VBM) states are derived mostly from the iodine $5p$ states while the conduction band minimum (CBM) states are primarily of Pb $6p$ character. The organic molecule derived electronic states are several eV below the band gap and show little dispersion, indicating negligible electronic coupling between the organic and organic components. Therefore, the organic molecules are not particularly relevant as far as the optical absorption is concerned. These results are consistent with previous theoretical work.[22,43–45] However, we would like to mention that organic molecules do affect significantly the low energy electronic structure of $MAPbI_3$ indirectly through a lattice distortion mechanism which will be discussed later.
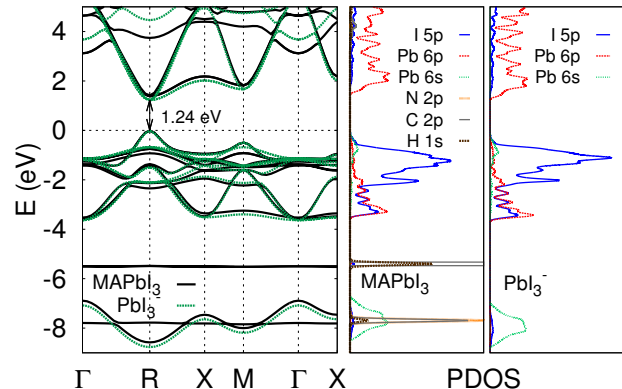
FIG. 4: (Color online) Band structures of cubic PbI_3^- (green dashed curve) and $MAPbI_3$ (black solid curve) with the corresponding projected density of states calculated using the PBE functional without including the SOC effects.

B. SELF-ENERGY AND SOC EFFECTS

Next we probe the quasiparticle self-energy and SOC effects on the low-energy (near the band-edge) electronic structure. Since the optically relevant electronic states are mostly derived from the inorganic framework, and the electronic coupling (hybridization) between organic and inorganic components is weak as shown in Fig. 4, we will focus our discussion on the PbI_3^- framework first.

Figure 5(a) compares the GW quasiparticle band structure of cubic PbI_3^- calculated with SOC (red solid lines) and without SOC (green dashed) effects. Without including the SOC effects, the calculated quasiparticle

band gap for cubic PbI_3^- is about $2.07\,\text{eV}$; with the SOC effect included, the quasiparticle band gap is reduced to about $0.93\,\text{eV}$. The strong SOC effect results in a very large splitting of the CBM states of about $1.5\,\text{eV}$ at the R point. Sizable spin-orbit splittings are also observed for valence bands located $2.5 \sim 3.5\,\text{eV}$ below the VBM since these states also have significant Pb-$6p$ components (see Fig. 4). A schematic band diagram is also shown in Fig. 5(b) to better illustrate the GW self-energy and SOC effects on the fundamental band gap of the cubic PbI_3^- framework. The GW self-energy correction increases the band gap by $0.83\,\text{eV}$ whereas the SOC effects reduce the band gap by $1.14\,\text{eV}$.
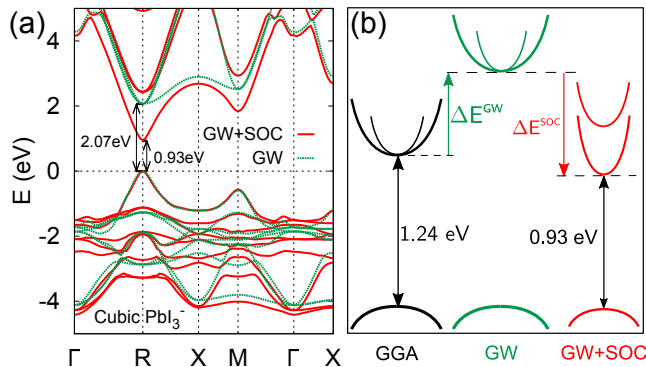
FIG. 5: (Color online) (a) Quasiparticle band structure of cubic PbI_3^- calculated without SOC corrections (green dashed curve) and with SOC corrections (red solid curve); (b) Schematic diagram (not plotted in scale) showing the quasiparticle self-energy (ΔE^{GW}) and SOC effects (ΔE^{SOC}).

The loss of inversion symmetry due to the presence of organic molecules results in addtional splitting (the Rashba-Dresselhaus SOC effect) to the otherwise spin-degenerate band structures. Figure 6 shows the band structure of cubic $MAPbI_3$ with the MA molecule oriented along the [011] direction. Compared wih Fig. 5, notable differences can be seen, in particular, the splitting of the spin states. The Rashba-Dresselhaus SOC effects in $MAPbI_3$ have also been discussed in previous works.[46–48]

Another notable effect of SOC on the calculated electronic structure is the reduction of the effective mass of the CBM and VBM states. The effective masses of cubic PbI_3^- calculated with different theoretical methods are summarized in Table I. The strong SOC effect significantly reduces the calculated effective masses, especially for the electron masses. The transverse electron mass is reduced by nearly one order of magnitude; for the longitudinal electron mass, the reduction is about 60%. These reduced carriers effective masses are beneficial for both high carrier mobility[35,37] and a small exciton-binding energy.[8]

We would like to mention that the calculated effective masses are sensitive to the structural models (e.g., cubic or tetragonal) used and the level of theoretical treatment (e.g., DFT vs the GW level, without or without the SOC
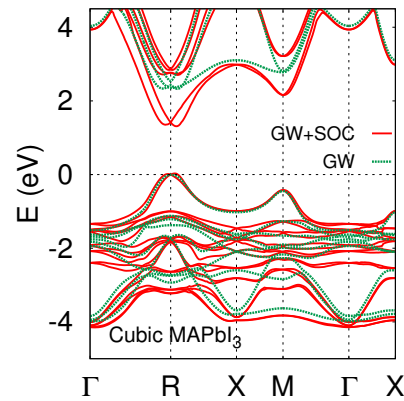
FIG. 6: Quasiparticle band structure of cubic $MAPbI_3$ showing the additional SOC splitting due to the loss of inversion symmetry.

effects, etc.). As a result, reported theoretical electron effective mass for the cubic phase ranges from $0.09\,m_0$ to $0.21\,m_0$,[7,36,49] and that for the tetragonal phase ranges from $0.14\,m_0$ to $0.29\,m_0$.[7,35,36] Our results are consistent with previous studies with different treatments of the spin-orbit coupling effects,[36,37,50] which also reported significantly reduced effective masses due to SOC.

TABLE I: Longitudinal and transverse effective masses for electron ($m_{e,L}$ and $m_{e,T}$) and hole ($m_{h,L}$ and $m_{h,T}$) states of cubic PbI_3^- calculated with different methods.

Method	$m_{e,L}$	$m_{e,T}$	$m_{h,L}$	$m_{h,T}$
DFT	0.19	0.74	0.12	0.12
G^0W^0	0.21	0.83	0.13	0.13
G^0W^0+SOC	0.08	0.08	0.09	0.09

C. EFFECTS OF ORGANIC MOLECULES AND STRUCTURAL DISTORTIONS

Although the chemical hybridization between the organic molecules and the inorganic framework is weak as discuss earlier, the organic part plays a pivotal role in defining the overall lattice parameters and stability of the system. In addition, the presence of MA molecules introduces substantial distortions to the PbI_3^- framework, which in turn may result in significant changes to the electronic structure by modifying the electronic coupling within the PbI_3^- framework. It was pointed out in a recent study that structural relaxations of the inorganic framework depend sensitively on the assumed direction of the organic molecules, and so does the calculated band gap.[51] Recent neutron scattering experiments[52] and first-principle calculations[53] also suggested sizable coupling between the inorganic framework and the organic cation. It should be pointed out that this coupling can be of both static and dynamic in nature, which, when combined

with temperature and electron-phonon (el-ph) renormalization effects, can greatly complicate theoretical understanding of the electronic properties of this material.

In this work, we will focus our discussion on the effects of the static structural distortions due to the presence of organic molecules. We would, however, like to comment on the temperature effects briefly. Temperature may affect the quasiparticle band gap of MAPbI$_3$ through various mechanisms. First, temperature may induce a volume change to the system. As these materials have a rather large thermal expansion coefficient, the temperature-dependent lattice constants will affect the band gap. We will come back to this point later. Second, at finite temperatures, organic molecules are essentially randomly oriented;[22–24] these randomly oriented organic molecules will affect the (static) structural distortions of the PbI$_3^-$ framework, which in turns will affect the band gap. Third, the renormalization of electron energy due to the el-ph coupling, which also depends on temperature, will certainly affect the band gap. Finally, temperature induced phase transition (e.g., from tetragonal to cubic) will modify the band gap. In the following, we will try to gauge the magnitudes and tendencies of the structural distortion (relaxation) effects brought by MA molecues.
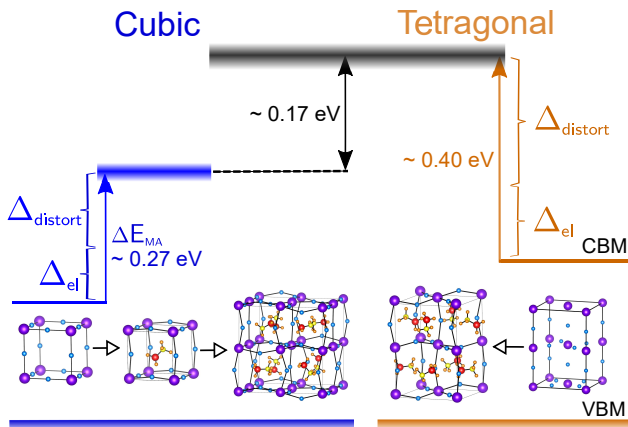
FIG. 7: (Color online) Schematic diagram summarizing the effects of organic molecules on the calculated band gap of MAPbI$_3$ at the DFT level. The random orientation of organic molecules and the associated structural distortions contribute significantly to enhancing the band gap of this material.

Figure 7 shows schematically the effects of organic molecules on the calculated (DFT) band gap at various levels. If a primitive cubic cell model is used, the presence of organic molecules results in about 0.27 eV increase in the calculated band gap at the DFT level. This increase in band gap may be further decomposed into a *direct* (electronic, Δ_{el}) and indirect (structural distortion, $\Delta_{distort}$) effects. The direct electronic contribution ($\Delta_{el} = 0.1$ eV) is defined as the difference in the calculated band gap between cubic PbI$_3^-$ and cubic MAPbI$_3$ without allowing the internal structure to relax, which reveals the direct electronic coupling between the organic molecules and the PbI$_3^-$ framework. Allowing structural

relaxations (while keeping the lattice constant fixed at experimental value) further increases the band gap by about 0.17 eV ($\Delta_{distort}$). Different orientations of the MA molecule result in slightly different results as shown in Table II. For the tetragonal phase, the calculated Δ_{el} is also about 0.1 eV, while $\Delta_{distort}$ is about 0.3 eV.

TABLE II: Calculated band gap (in eV) of MAPbI$_3$: Effects of MA molecules and structural distortions and comparision with experiments.

Phase	Structure		E_g^{PBE}	E_g^{GW+SOC}
Cubic (primitive)	PbI$_3^-$	ideal struct.	1.24	0.93
	MAPbI$_3$	MA [001]	1.54	1.43
		MA [011]	1.51	1.40
		MA [111]	1.47	1.31
Tetragonal (primitive)	MAPbI$_3$	MA [001]	1.68	1.67
		MA [011]	1.76	1.73
		MA [111]	1.76	1.72
C & T (supercell)	MAPbI$_3$	with MA directions randomized	1.68± 0.08	1.65± 0.08
Experiment	MAPbI$_3$	1.51~1.66 Refs.[17,22,26,54–56]		

The use of cubic primitive cells brings in artificial polarization effects and greatly limits the degrees of freedom for structural relaxation. As we mentioned earlier, organic molecules are essentially randomly oriented in synthesized materials.[22–24] These randomly oriented organic molecules result in greater degrees of freedom for structural relaxations (distortions). The distortions to the PbI$_3^-$ framework in turns modifies the electronic coupling within the inorganic framework, thus affecting the calculated band gap. To this end, we have created $2\times2\times2$ supercells for the cubic phase and placed MA molecules in random directions. As it is shown in Fig. 7, the PbI$_3^-$ framework is now significantly distorted. These enhanced structural distortions further contribute to about 0.17 eV in the calculated band gap at the DFT level (see Fig. 7 and Table II). This result is obtained by averaging over 10 supercell structures with MA molecules randomly oriented. We mention that notable distortions to the inorganic framework have also been observed experimentally.[57]

Since the primitive cell of the tetragonal phase is already 4 times that of the cuibc phase, which is large enough for modeling random orientations of organic molecules, we did not create supercells for the tetragonal phase. We have, however, calculated the band gap for 10 tetragonal structures with MA molecules randomly oriented. The calculated band gap for tetragonal model structures with MA molecules randomly oriented does not vary significant cross all structure models, and it turns out that the averaged band gap calculated for optimized tetrahonal structures (with MA molecules randomly oriented) is similar (within 0.05 eV) to that for cubic supercells. Our results also agree with ex-

periments that there the change in the measured band gap is negligible (~ 0.01 eV) across the phase transition temperature.[51,54–56]. Our results on the strong effects of structural distortions on the calculated band gap also agree with previous theoretical works.[51,58].

Putting all results together, we estimate that the DFT band gap of MAPbI$_3$ is about 1.68 ± 0.08 eV (Table II). The uncertainty comes from the variations of the calculated band gap using different structural models. Table II also summarizes the GW+SOC results for various structural models. Adding the averaged GW+SOC corrections to the DFT results for the tetragonal phase, our best estimate for the quasiparticle band gap (including SOC effects) for MAPbI$_3$ is 1.65 ± 0.08 eV. Our final results are consistent with earlier theoretical works.[35,36,51] These results also compare well with the measured optical band gap of about $1.51 \sim 1.66$ eV.[17,22,26,54–56] We mention that the el-ph renormalization effects (which tend to reduce the band gap with increasing temperature) are not included in our calculation as we have mentioned earlier. As a reference, the el-ph renormalization is about 0.15 eV[59] in ZnO due to zero-point vibrations. Excitonic effects (i.e., electron-hole interaction), on the other hand, are expected to be weak in this material; a recent experiment[60] reports a small exciton binding energy of about 16 meV at low temperatures. At room temperature, the exciton binding energy is reduced to only a few meV.

D.   EFFECTS OF LATTICE CONSTANTs
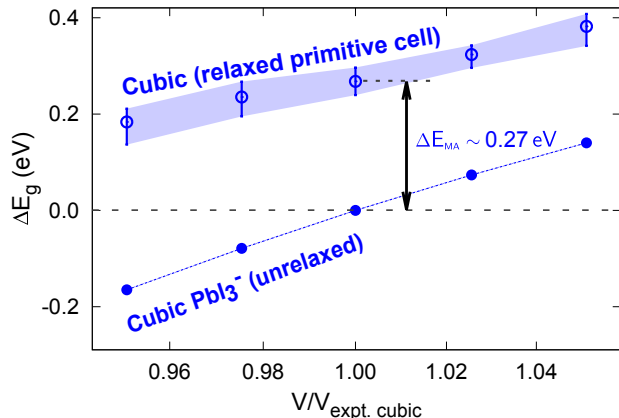
FIG. 8: Calculated (DFT) band gap of MAPbI$_3$ as a function of cell volume. The error bars and the shaded area represent the fluctuation of the band gap calculated by placing the MA molecules along [001], [011] and [111] directions.

We now discuss briefly the effects of lattice constants on the electronic structure of MAPbI$_3$. The lattice constants (cell volume) of organometal perovskites can be affected/tuned by various means such as temparature,[22] replacing methylammonium with different organic cations,[17,19] or mechanical strains in-

duced by substrates.[10] Previous theoretical studies have shown a positive band gap deformation potential ($a_V = \partial E_g / \partial \ln V$) of these materials.[61] We would like to point out, however, that one cannot compare directly the calculated volume-dependent band gap with the measured temperature-dependent band gap[54–56] by simply taking into account the thermal expansion effects. This is because the temperature-dependent el-ph effects (which tend to reduce the band gap with increasing temperature[62]) cancel out partially the volume deformation effects (which tend to increase the band gap with increasing temperature as a result of thermal expansion and a positive deformation potential).

Figure 8 shows the calculated volume-dependent band gap of cubic PbI$_3^-$ and cubic MAPbI$_3$ at the DFT level using the band gap of cubic PbI$_3^-$ as a reference. For cubic MAPbI$_3$, internal atomic coordinates are fully relaxed while keeping the the lattice constant fixed for a given volume. For each cell volume, the band gap of cubic MAPbI$_3$ is calculated with three different orientations (i.e., along [001], [011] and [111] directions) of the organic molecules. The calculated band gap deformation potential is 3.0 eV for PbI$_3^-$ and 2.1 eV for cubic MAPbI$_3$ at the DFT level. The positive deformation potential can be understood in terms of the enhanced atomic orbital interaction (thus greater dispersion) with decreasing cell volume, resulting in the lowering of the CBM and rising of the VBM states. If we use the measured thermal expansion coefficient[22] and the temperature-dependent band gap[54] for the cubic phase, we estimated that the *apparent* experimental deformation potential be around 1.5 eV. This is substantially smaller than the calculated value of 2.1 eV. The discrepancy may be resolved by taking into account the el-ph renormalization effects, which tend to reduce the band gap with increasing temperature as discussed earlier.

IV.   CONCLUSION

In conclusion, we have analyzed the effects of several major factors, namely, quasiparticle self-energy, spin-orbit coupling, the organic cation, and structural distortions on the electronic structure of MAPbI$_3$. Although the band-edge states are derived primarily from the inorganic framework with negligibly small hybridizations with organic molecules, organic molecules indirectly affect the band gap by introducing distortions to the inorganic cage and controlling the overall lattice constants.

The quasiparticle band gap of cubic PbI$_3^-$ calculated with experimental lattice parameters is 0.93 eV including the GW self-energy and SOC effects. Including organic molecules and allowing the structure to relax within a primitive cubic cell increase the band gap to about 1.4 eV. When supercells are used, which allow greater degrees of freedom for atomic relaxation, the quasiparticle band gap increases to 1.65 ± 0.08 eV, with the undertainty coming from different structural models with ran-

dom orientations of the MA molecules. Our results compare favorably with measured values ranging from 1.51 to 1.66 eV.[17,22,26,54–56] The SOC coupling drastically reduces the band gap and the electron and hole effective masses of these materials. We illustrate that the electronic structures of complex materials can be better understood by investigating into the role of each controlling factor. Our results may serve as a guidance for future optimization of related organometal perovskite photovoltaic materials.

V. ACKNOWLEDGEMENT

[*] Electronic address: pzhang3@buffalo.edu

[1] H. Zhou, Q. Chen, G. Li, S. Luo, T.-b. Song, H.-S. Duan, Z. Hong, J. You, Y. Liu, and Y. Yang, Science **345**, 542 (2014).

[2] M. A. Green, A. Ho-Baillie, and H. J. Snaith, Nature Photonics **8**, 506 (2014).

[3] M. M. Lee, J. Teuscher, T. Miyasaka, T. N. Murakami, and H. J. Snaith, Science **338**, 643 (2012).

[4] S. De Wolf, J. Holovsky, S.-J. Moon, P. Lper, B. Niesen, M. Ledinsky, F.-J. Haug, J.-H. Yum, and C. Ballif, The Journal of Physical Chemistry Letters **5**, 1035 (2014).

[5] G. Xing, N. Mathews, S. Sun, S. S. Lim, Y. M. Lam, M. Grtzel, S. Mhaisalkar, and T. C. Sum, Science **342**, 344 (2013).

[6] S. D. Stranks, G. E. Eperon, G. Grancini, C. Menelaou, M. J. P. Alcocer, T. Leijtens, L. M. Herz, A. Petrozza, and H. J. Snaith, Science **342**, 341 (2013).

[7] Y. Wang, Y. Zhang, P. Zhang, and W. Zhang, Phys. Chem. Chem. Phys. **17**, 11516 (2015).

[8] Q. Lin, A. Armin, R. C. R. Nagiri, P. L. Burn, and P. Meredith, Nature Photonics **9**, 106 (2015), article, URL http://dx.doi.org/10.1038/nphoton.2014.284.

[9] K. Tanaka, T. Takahashi, T. Ban, T. Kondo, K. Uchida, and N. Miura, Solid State Communications **127**, 619 (2003).

[10] J. Feng, APL Materials **2**, 081801 (2014).

[11] N. K. Noel, S. D. Stranks, A. Abate, C. Wehrenfennig, S. Guarnera, A.-A. Haghighirad, A. Sadhanala, G. E. Eperon, S. K. Pathak, M. B. Johnston, et al., Energy Environ. Sci. **7**, 3061 (2014).

[12] M. H. Kumar, S. Dharani, W. L. Leong, P. P. Boix, R. R. Prabhakar, T. Baikie, C. Shi, H. Ding, R. Ramesh, M. Asta, et al., Advanced Materials **26**, 7122 (2014).

[13] Y.-Y. Sun, J. Shi, J. Lian, W. Gao, M. L. Agiorgousis, P. Zhang, and S. Zhang, Nanoscale pp. – (2016), URL http://dx.doi.org/10.1039/C5NR04310G.

[14] Y.-Y. Sun, M. L. Agiorgousis, P. Zhang, and S. Zhang, Nano Letters **15**, 581 (2015), URL http://dx.doi.org/10.1021/nl504046x.

[15] S. A. Kulkarni, T. Baikie, P. P. Boix, N. Yantara, N. Mathews, and S. Mhaisalkar, J. Mater. Chem. A **2**, 9221 (2014).

[16] Y. Chen, T. Chen, and L. Dai, Advanced Materials **27**, 1053 (2015).

[17] G. E. Eperon, S. D. Stranks, C. Menelaou, M. B. Johnston, L. M. Herz, and H. J. Snaith, Energy Environ. Sci. **7**, 982 (2014).

[18] N. J. Jeon, J. H. Noh, W. S. Yang, Y. C. Kim, S. Ryu, J. Seo, and S. I. Seok, Nature **517**, 476 (2015).

[19] M. R. Filip, G. E. Eperon, H. J. Snaith, and F. Giustino, Nature Communications **5** (2014).

[20] M. S. Hybertsen and S. G. Louie, Phys. Rev. B **34**, 5390 (1986).

[21] Y. Kawamura, H. Mashiyama, and K. Hasebe, Journal of the Physical Society of Japan **71**, 1694 (2002).

[22] T. Baikie, Y. Fang, J. M. Kadro, M. Schreyer, F. Wei, S. G. Mhaisalkar, M. Graetzel, and T. J. White, J. Mater. Chem. A **1**, 5628 (2013).

[23] N. Onoda-Yamamuro, T. Matsuo, and H. Suga, Journal of Physics and Chemistry of Solids **51**, 1383 (1990), ISSN 0022-3697.

[24] M. T. Weller, O. J. Weber, P. F. Henry, A. M. Di Pumpo, and T. C. Hansen, Chem. Commun. **51**, 4180 (2015).

[25] A. Poglitsch and D. Weber, The Journal of Chemical Physics **87**, 6373 (1987).

[26] C. C. Stoumpos, C. D. Malliakas, and M. G. Kanatzidis, Inorganic Chemistry **52**, 9019 (2013).

[27] W. Kohn and L. J. Sham, Phys. Rev. **140**, A1133 (1965).

[28] P. Giannozzi, S. Baroni, N. Bonini, M. Calandra, R. Car, C. Cavazzoni, D. Ceresoli, G. L. Chiarotti, M. Cococcioni, I. Dabo, et al., Journal of Physics: Condensed Matter **21**, 395502 (2009).

[29] Accessed: 2015-07-28, URL http://www.nersc.gov/users/software/applications/materials-science/paratec/.

[30] J. P. Perdew, K. Burke, and M. Ernzerhof, Phys. Rev. Lett. **77**, 3865 (1996).

[31] N. Troullier and J. L. Martins, Phys. Rev. B **43**, 1993 (1991).

[32] H. J. Monkhorst and J. D. Pack, Phys. Rev. B **13**, 5188 (1976).

[33] J. Deslippe, G. Samsonidze, D. A. Strubbe, M. Jain, M. L. Cohen, and S. G. Louie, Computer Physics Communications **183**, 1269 (2012).

[34] M. S. Hybertsen and S. G. Louie, Phys. Rev. B **34**, 2920

(1986).

[35] E. M. Paolo Umari and F. D. Angelis, Scientific Reports **4** (2014).

[36] F. Brivio, K. T. Butler, A. Walsh, and M. van Schilfgaarde, Phys. Rev. B **89**, 155204 (2014).

[37] M. R. Filip and F. Giustino, Phys. Rev. B **90**, 245145 (2014).

[38] B. D. Malone and M. L. Cohen, Journal of Physics: Condensed Matter **25**, 105503 (2013).

[39] B.-C. Shih, Y. Xue, P. Zhang, M. L. Cohen, and S. G. Louie, Phys. Rev. Lett. **105**, 146401 (2010), URL `http://link.aps.org/doi/10.1103/PhysRevLett.105.146401`.

[40] C. Friedrich, M. C. Müller, and S. Blügel, Phys. Rev. B **83**, 081101 (2011), URL `http://link.aps.org/doi/10.1103/PhysRevB.83.081101`.

[41] A. A. Mostofi, J. R. Yates, Y.-S. Lee, I. Souza, D. Vanderbilt, and N. Marzari, Computer Physics Communications **178**, 685 (2008).

[42] I. Souza, N. Marzari, and D. Vanderbilt, Phys. Rev. B **65**, 035109 (2001), URL `http://link.aps.org/doi/10.1103/PhysRevB.65.035109`.

[43] F. Brivio, A. B. Walker, and A. Walsh, APL Mater. **1**, 042111 (2013), URL `http://scitation.aip.org/content/aip/journal/aplmater/1/4/10.1063/1.4824147`.

[44] E. Mosconi, A. Amat, M. K. Nazeeruddin, M. Grtzel, and F. D. Angelis, The Journal of Physical Chemistry C **117**, 13902 (2013).

[45] I. Borriello, G. Cantele, and D. Ninno, Phys. Rev. B **77**, 235214 (2008), URL `http://link.aps.org/doi/10.1103/PhysRevB.77.235214`.

[46] C. Motta, F. El-Mellouhi, S. Kais, N. Tabet, F. Alharbi, and S. Sanvito, Nature communications **6** (2015).

[47] M. Kepenekian, R. Robles, C. Katan, D. Sapori, L. Pedesseau, and J. Even, ACS Nano (2015).

[48] J. Even, L. Pedesseau, C. Katan, M. Kepenekian, J.-S. Lauret, D. Sapori, and E. Deleporte, The Journal of Physical Chemistry C **119**, 10161 (2015).

[49] Y. He and G. Galli, Chemistry of Materials **26**, 5394 (2014).

[50] J. Even, L. Pedesseau, J.-M. Jancu, and C. Katan, physica status solidi (RRL) - Rapid Research Letters **8**, 31 (2014).

[51] C. Quarti, E. Mosconi, J. M. Ball, V. D'Innocenzo, C. Tao, S. Pathak, H. J. Snaith, A. Petrozza, and F. De Angelis, Energy Environ. Sci. (2015), URL `http://dx.doi.org/10.1039/C5EE02925B`.

[52] I. P. Swainson, C. Stock, S. F. Parker, L. Van Eijck, M. Russina, and J. W. Taylor, Phys. Rev. B **92**, 100303 (2015), URL `http://link.aps.org/doi/10.1103/PhysRevB.92.100303`.

[53] F. Brivio, J. M. Frost, J. M. Skelton, A. J. Jackson, O. J. Weber, M. T. Weller, A. R. Goñi, A. M. A. Leguy, P. R. F. Barnes, and A. Walsh, Phys. Rev. B **92**, 144308 (2015), URL `http://link.aps.org/doi/10.1103/PhysRevB.92.144308`.

[54] R. L. Milot, G. E. Eperon, H. J. Snaith, M. B. Johnston, and L. M. Herz, Advanced Functional Materials **25**, 6218 (2015), URL `http://dx.doi.org/10.1002/adfm.201502340`.

[55] B. J. Foley, D. L. Marlowe, K. Sun, W. A. Saidi, L. Scudiero, M. C. Gupta, and J. J. Choi, Applied Physics Letters **106**, 243904 (2015), URL `http://scitation.aip.org/content/aip/journal/apl/106/24/10.1063/1.4922804`.

[56] T. Dittrich, C. Awino, P. Prajongtat, B. Rech, and M. C. Lux-Steiner, The Journal of Physical Chemistry C **119**, 23968 (2015), http://dx.doi.org/10.1021/acs.jpcc.5b07132, URL `http://dx.doi.org/10.1021/acs.jpcc.5b07132`.

[57] R. J. Worhatch, H. Kim, I. P. Swainson, A. L. Yonkeu, and S. J. L. Billinge, Chemistry of Materials **20**, 1272 (2008), URL `http://dx.doi.org/10.1021/cm702668d`.

[58] A. M. A. Leguy, P. Azarhoosh, M. I. Alonso, M. Campoy-Quiles, O. J. Weber, J. Yao, D. Bryant, M. T. Weller, J. Nelson, A. Walsh, et al., Nanoscale pp. – (2016), URL `http://dx.doi.org/10.1039/C5NR05435D`.

[59] S. Tsoi, X. Lu, A. K. Ramdas, H. Alawadhi, M. Grimsditch, M. Cardona, and R. Lauck, Phys. Rev. B **74**, 165203 (2006), URL `http://link.aps.org/doi/10.1103/PhysRevB.74.165203`.

[60] A. Miyata, A. Mitioglu, P. Plochocka, O. Portugall, J. T.-W. Wang, S. D. Stranks, H. J. Snaith, and R. J. Nicholas, Nature Physics **11**, 582 (2015), article, URL `http://dx.doi.org/10.1038/nphys3357`.

[61] J. M. Frost, K. T. Butler, F. Brivio, C. H. Hendon, M. van Schilfgaarde, and A. Walsh, Nano Letters **14**, 2584 (2014).

[62] F. Giustino, S. G. Louie, and M. L. Cohen, Phys. Rev. Lett. **105**, 265501 (2010), URL `http://link.aps.org/doi/10.1103/PhysRevLett.105.265501`.